A&A 678, A56 (2023)
https://doi.org/10.1051/0004-6361/202346777

Astronomy & Astrophysics

Probing magnetic fields in the circumgalactic medium using polarization data from MIGHTEE

K. Böckmann[1], M. Brüggen[1], V. Heesen[1], A. Basu[2], S. P. O'Sullivan[3], I. Heywood[4,5,6], M. Jarvis[7,8], A. Scaife[9,10], J. Stil[11], R. Taylor[12], N. J. Adams[9], R. A. A. Bowler[9], and M. N. Tudorache[7]

[1] Hamburger Sternwarte, Universität Hamburg, Gojenbergsweg 112, 21029 Hamburg, Germany
e-mail: Kathrin.Boeckmann@hs.uni-hamburg.de
[2] Thüringer Landessternwarte, Sternwarte 5, 07778 Tautenburg, Germany
[3] Departamento de Física de la Tierra y Astrofísica & IPARCOS-UCM, Universidad Complutense de Madrid, 28040 Madrid, Spain
[4] Astrophysics, Department of Physics, University of Oxford, Keble Road, Oxford OX1 3RH, UK
[5] Department of Physics and Electronics, Rhodes University, PO Box 94, Makhanda 6140, South Africa
[6] South African Radio Astronomy Observatory, 2 Fir Street, Observatory 7925, South Africa
[7] Astrophysics, Department of Physics, University of Oxford, Keble Road, Oxford OX1 3RH, UK
[8] National Radio Astronomy Observatory, 1003 Lopezville Road, Socorro, NM 87801, USA
[9] Jodrell Bank Centre for Astrophysics, University of Manchester, Oxford Road, M13 9PL Manchester, UK
[10] The Alan Turing Institute, Euston Road, London NW1 2DB, UK
[11] Department of Physics and Astronomy, The University of Calgary, 2500 University Drive NW, Calgary, AB T2N 1N4, Canada
[12] Inter-University Institute for Data Intensive Astronomy, and Department of Astronomy, University of the Western Cape, 7535 Bellville, South Africa

Received 29 April 2023 / Accepted 29 August 2023

ABSTRACT

Context. The properties and evolution of magnetic fields surrounding galaxies are observationally largely unconstrained. The detection and study of these magnetic fields is important to understand galaxy evolution since magnetic fields are tracers for dynamical processes in the circumgalactic medium (CGM) and can have a significant impact on the evolution of the CGM.
Aims. The Faraday rotation measure (RM) of the polarized light of background radio sources passing through the magnetized CGM of intervening galaxies can be used as a tracer for the strength and extent of magnetic fields around galaxies.
Methods. We used rotation measures observed by the MIGHTEE-POL (MeerKAT International GHz Tiered Extragalactic Exploration polarization) survey by MeerKAT in the XMM-LSS and COSMOS fields to investigate the RM around foreground star-forming galaxies. We used spectroscopic catalogs of star-forming and blue cloud galaxies to measure the RM of MIGHTEE-POL sources as a function of the impact parameter from the intervening galaxy. In addition, we examined the dependence of the RM on redshift. We then repeated this procedure using a deeper galaxy catalog with photometric redshifts.
Results. For the spectroscopic star-forming sample, we find a redshift-corrected |RM| excess of $5.6 \pm 2.3\,\mathrm{rad\,m^{-2}}$ which corresponds to a 2.5σ significance around galaxies with a median redshift of $z = 0.46$ for impact parameters below 130 kpc only selecting the intervenor with the smallest impact parameter. Making use of a photometric galaxy catalog and taking into account all intervenors with $M_g < -13.6$ mag, the signal disappears. We find no indication for a correlation between redshift and RM, nor do we find a connection between the total number of intervenors to the total |RM|.
Conclusions. We have presented tentative evidence that the CGM of star-forming galaxies is permeated by coherent magnetic fields within the virial radius. We conclude that mostly bright, star-forming galaxies with impact parameters less than 130 kpc significantly contribute to the RM of the background radio source.

Key words. galaxies: fundamental parameters – galaxies: magnetic fields – radio continuum: galaxies – galaxies: ISM

1. Introduction

The diffuse gas embedded between the interstellar medium (ISM) and the baryon-rich intergalactic medium (IGM) of a galaxy is known as the circumgalactic medium (CGM), which typically extends up to the virial radius of galaxies ≈200 kpc. The existence of this extended gaseous halo is a fundamental prediction of galaxy formation theory (e.g., Tumlinson et al. 2017). Observations and simulations from across the whole electromagnetic spectrum and redshifts suggest that the CGM gas has a major impact on galaxy evolution and on the chemical history and evolution of a galaxy (e.g., Donahue & Voit 2022). Firstly, it receives enriched material that was expelled in the form of outflows; secondly, it also acts as a reservoir of fuel for future star formation, including the infalling IGM gas (Machado et al. 2018). One powerful tool that is used to study the tenuous multiphase CGM are transverse absorption-line studies using background quasars, which enables one to determine the relative abundance of various elements and thus the metallicity of the gas (Mintz et al. 2020; DeFelippis et al. 2021).

Magnetic fields are an important non-thermal component in and around galaxies that affect the dynamics and structure of the CGM. In particular, they are believed to play an important role in the transport of materials to and from disks into the CGM (Arámburo-García et al. 2023) and affect how gas is accreted onto galaxies (Heesen et al. 2023). However, little is

known about the dynamical importance of the magnetic fields and their evolution in galaxies and the surrounding CGM over cosmic time. Moreover, it is not yet understood how the CGM gets magnetized in the first place. Two possible scenarios have been discussed: (i) magnetic fields could be generated by small-scale dynamo effects (Pakmor et al. 2017, 2020) and (ii) magnetic fields could be generated in the disk and subsequently transported out via galactic winds and outflows (Péroux et al. 2020). In the former case, we expect the resulting magnetic fields to be turbulent with no ordered fields on the size of the CGM. However, the turbulent magnetic fields can be converted to anisotropic fields by shear flows (Fletcher et al. 2011). If galactic winds and feedback are the origin of the magnetized CGM, a strong azimuthal dependence with the galactic disk is expected because the outflows are usually along the minor axis. This is valid for both, stellar and AGN (Active Galatic Nuclei) driven feedback (Thomas et al. 2022; Pillepich et al. 2021).

Magnetic fields in nearby (distance < 50 Mpc) star-forming disk galaxies have been studied in some detail, with most studies indicating the existence of a galactic dynamo (Beck et al. 1996; Beck 2015). For more distant galaxies at redshift $z > 0.1$, the data is scarcer with only a few studies existing (Oren & Wolfe 1995; Bernet et al. 2008; Farnes et al. 2014; Kim et al. 2016; Mao et al. 2017; Lan & Prochaska 2020). Measuring the magnetic fields directly via synchrotron emission is usually limited to regions close to the galactic disk due to spectral aging (Miskolczi et al. 2019). Hence, the direct mapping of the magnetic field structure and strength in galaxies at higher redshifts will be a challenging and important task for the next generation of radio telescopes, such as the Square Kilometre Array (SKA).

In this paper we use Faraday rotation to examine the magnetic fields around galaxies. Faraday rotation is a process that rotates the polarization angle of linearly polarized light when passing through an ionized and magnetized medium. The intervening medium causes a difference in the phase velocity between the left-handed and right-handed circular polarization components of the linearly polarized synchrotron radiation. Using the polarization angle ψ, the observed wavelength λ and the Faraday depth ϕ, the Faraday rotation can be described by a rotation of the intrinsic polarization angle:

$$\psi(\lambda^2) = \psi_0 + \phi\lambda^2. \tag{1}$$

The Faraday rotation measure (RM) modifies the polarization angle via

$$\psi(\lambda) = \psi_0 + \mathrm{RM}\lambda^2. \tag{2}$$

Faraday rotation of distant background radio sources has been used to probe extragalactic magnetic fields (Pomakov et al. 2022). The RM of the polarized light from background radio sources passing through the magnetized CGM can be used as a tracer of the strength and extent of magnetic fields around galaxies out to distances of hundreds of kiloparsecs. The RM is assumed to be positive when the line-of-sight average component of the magnetic field points toward the observer, otherwise it is negative for a field with an average component pointing away from the observer (Vacca et al. 2016). For a polarized radio source at redshift z, the RM is defined as

$$\frac{\mathrm{RM}}{\mathrm{rad\,m^{-2}}} = 0.81 \int_z^0 \frac{1}{(1+z)^2} \left(\frac{n_\mathrm{e}(z)}{\mathrm{cm^{-3}}}\right)\left(\frac{B_\parallel(z)}{\mu\mathrm{G}}\right)\left(\frac{\mathrm{d}r(z)}{\mathrm{d}z}\right)\mathrm{d}z. \tag{3}$$

The RM has units of rad m^{-2}, the free electron number density n_e is in cm^{-3}, the magnetic field component along the line of sight $B_\parallel$ is in Gauss and the comoving path increment per unit redshift $\mathrm{d}l/\mathrm{d}z$ is in parsec. This equation assumes a uniform RM screen across the source and a spatial separation of the linearly polarized source and the Faraday rotating plasma (Akahori et al. 2016; Bernet et al. 2012).

Previous work has studied the Faraday rotation properties of background quasars with strong intervening Mg II lines in their spectra. Mg II absorption is usually associated with the halos of normal galaxies. The absolute values of RM are found to be correlated with the presence of intervening Mg II absorption, which is thought to arise in outflowing material from star forming galaxies (Kacprzak et al. 2008; Kim et al. 2016). Work of Bernet et al. (2008, 2010) showed that Mg II absorbers exhibit the highest |RM| at frequencies of 5 GHz and above. At lower frequencies, the effect of Faraday depolarization becomes stronger because the Faraday rotation is proportional to the square of the wavelength (Eq. (1)). Bernet et al. (2013) examined the |RM| distribution with respect to the impact parameters of galaxies finding that all sightlines with high |RM| pass within 50 kpc of a galaxy and that the |RM| distribution for low impact parameters, $D < 50$ kpc, is significantly different than for larger impact parameters. Farnes et al. (2014) examined 1.4 GHz data of 599 optically identified non-intrinsic MgII absorption systems with polarized background radio sources finding that the excess of |RM| is still present in that frequency range but only for sources where the impact parameters between the quasar and the polarized emission are small.

Recently, Heesen et al. (2023) studied the residual rotation measures (RRMs) observed with the LOw Frequency ARray (LOFAR) around 183 nearby galaxies of the Palomar survey that were selected by apparent b-band magnitude (Carretti et al. 2023). Since Faraday rotation is proportional to the wavelength squared, LOFAR high-band frequencies (144 MHz in this study) afford high-precision RM measurements (O'Sullivan et al. 2023) at the cost of smaller source densities owing to depolarization. This work showed, for the first time, an RM along the minor axis of inclined galaxies for impact parameters of less than 100 kpc. These results suggest a slow decrease of the magnetic field strength with distance from the galactic disk, as expected if the CGM is magnetized by galactic winds and outflows. We note that this work focuses on nearby galaxies that are believed to have a smaller fraction of star-formation driven outflows than at higher redshifts.

Here, we measure the RM around foreground star-forming galaxies using early-release data from the MeerKAT MIGH- TEE polarization survey (MIGHTEE-POL, Taylor et al., in prep.) with the aim to measure the rotation measure profile out to distances of 300–400 kpc from the star-forming galaxies. This provides information about the magnetic fields in the CGM and galactic winds. We use catalogs of star-forming and blue cloud galaxies to measure the rotation measure of MIGHTEE-POL sources as a function of the impact parameter from the foreground galaxy. We use catalogs of star-forming galaxies since RMs are expected to be higher around star-forming galaxies than around quiescent galaxies. This is due to the fact that the interstellar medium in star-forming galaxies is more turbulent and magnetized, which leads to an increase of the RM. Star formation processes, such as supernova explosions and outflows from young stars, can amplify the magnetic field and drive magnetized outflows on galactic scales (Wiener et al. 2017; Basu et al. 2018).

This paper is organized as follows: In Sect. 2 we describe the data and our sample selection and describe the methods in Sect. 3. We present the results in Sect. 4 and discuss them in Sect. 5. We close with a conclusion in Sect. 6.

2. Data

The MIGHTEE survey (MeerKAT International GHz Tiered Extragalactic Exploration, Jarvis et al. 2016) is a survey that is being conducted using the MeerKAT radio telescope in South Africa. It is one of MeerKAT's flagship Large Survey Projects, using simultaneous continuum, spectropolarimetry (Sekhar et al. 2022) and spectral line (Maddox et al. 2021) measurements to investigate the formation and evolution of galaxies over cosmic time (Heywood et al. 2022). The MIGHTEE survey is imaging four extragalactic fields, Cosmic Evolution Survey (COSMOS; Scoville et al. 2007), XMM Large-Scale Structure survey (XMM-LSS; Pierre et al. 2004), CDFS, and ELAIS-S1. All fields are observed at L-band from 880–1680 MHz, with a central frequency of 1284 MHz in multiple pointings that are mosaicked to a final image with a thermal noise sensitivity of approximately 2 µJy beam^{-1}. In this work we make use of early-release data products from the MeerKAT MIGHTEE polarization survey (MIGHTEE-POL; Taylor et al., in prep.). The MIGHTEE-POL survey aims to study the polarized emission from extragalactic radio sources and the properties of magnetic fields in the Cosmic Web including the large-scale structure. The survey will cover an area of about 20 square degrees of the sky, with a resolution of ≈5 arcsec. The survey is expected to be completed in 2023 and the data will be made publicly available to the scientific community. In this work, we use continuum data early-release products from the MIGHTEE-POL survey of the COSMOS and XMM-LSS fields. The visibility data were calibrated and imaged in full polarization mode on the `ilifu` cloud facility using the CASA-based IDIA pipeline[1]. The analysis of the polarization signals was restricted to frequencies below 1380 MHz in order to minimize instrumental polarization effects. Below this frequency, the instrumental leakage for the MeerKAT remains below 0.2% within 0.5° of the field center.

Faraday depth spectra were computed at the location of sources detected in the total intensity catalog by applying the technique of RM synthesis on the fractional Stokes Q, U data between 886 and 1380 MHz with a channel resolution of 2.51 MHz. The rotation measure transfer function in these data has a typical width of 56 rad m^{-2} and the data are sensitive to Faraday depth of up to ±5000 rad m^{-2}. However, polarized emission was only searched over a Faraday depth range of ±2000 rad m^{-2}. The RM values used in this study were obtained from the location of the strongest polarized component in the Faraday depth spectrum. The RM were also estimated by modeling the frequency spectra of Stokes Q and U parameters, and the best-fit RM values were consistent with those obtained from the peak of the Faraday depth spectra within 1σ (Taylor et al., in prep.). Therefore, we do not expect the values of RM used in this work to be affected by spurious peaks in the Faraday depth spectrum origination due to Faraday complexity (Kim et al. 2016).

The COSMOS field consists of one pointing, for the XMM-LSS field three pointings are mosaicked together. The MIGHTEE-POL catalog of the XMM-LSS field consists of 243 sources and the catalog of the COSMOS field consists of 111 sources. For a more detailed description about the method of data processing see (Taylor et al., in prep.). Compared to lower frequency observations, e.g. with LOFAR, our polarized source density is higher because depolarization is lower. The flip side is that our individual RM values are less accurate as the angle shift depends on λ^2. In our data the average error on the RM is RM$_{\rm err}$ = 2.4 rad m^{-2}.

[1] https://idia-pipelines.github.io/docs/processMeerKAT

The redshift distribution of the host sources is shown in the upper panel of Fig. 1. In order to identify intervening galaxies in the XMM-LSS field we use the "blue cloud" galaxy catalog from Basu et al. (2015). This catalog consists of 36 776 blue galaxies with their spectroscopic redshifts from the PRism MUltiobject Survey (PRIMUS) up to a redshift of $z = 1.18$. A color–magnitude diagram based separation was introduced to only select blue star-forming galaxies. Furthermore, the PRIMUS team identified the AGN in their sample by fitting AGN spectral templates to remove AGN from the normal galaxy sample. In this catalog, due to the evolving main-sequence, high-z blue cloud galaxies tend to be luminous infrared galaxies (LIRGs) and ultra-luminous infrared galaxies (ULIRGs), and therefore dominated by mergers.

For the COSMOS field we use the galaxy catalog provided by Sinigaglia et al. (2022). This sample was derived from the parent sample by Weaver et al. (2022). A color–color $NUV-r/r-J$ plane selection was applied to only select star-forming galaxies. This catalog contains 9022 star-forming galaxies and their spectroscopic redshifts between $0.23 < z < 0.48$. We note that this sample is the result of the combination of several different surveys, performed with different survey strategies (Weaver et al. 2022; Davies et al. 2018). The distribution of the locations of intervening and host galaxies across the sky for both fields is shown in Fig. 2. We can see that the optical survey used in the catalog creation for the XMM-LSS field has a smaller footprint than the MIGHTEE survey. This reduces the size of the XMM-LSS field.

In addition to the two spectroscopic galaxy catalogs we also make use of two photometric galaxy catalogs (one for each field) provided by Hatfield et al. (2022). These catalogs were computed with optical and near-infrared data from VISTA and HyperSuprimeCam (VISTA Deep Extragalactic Observations, VIDEO: Jarvis et al. 2013; HSC: Aihara et al. 2018). We remove sources without redshift and magnitudes and implement a cut on the apparent Ks magnitude of $m_K < 23.7$. The magnitude cut is introduced to ensure uniformity and comparability between the two catalogs, given that the initial depth of the COSMOS catalog exceeds that of the XMM-LSS catalog by 1 mag. After doing so, we are left with 125 676 sources for the COSMOS field and 384 354 sources for the XMM-LSS field. The redshift range for the COSMOS field is $0.001 < z < 5.65$ with a median g-band magnitude of $M_g = -19.1$ mag. For the XMM-LSS we get $0.0001 < z < 6.45$ a median g-band magnitude of $M_g = -20.3$ mag. We use these catalogs to find the total number of intervenors to each host galaxy and to test for a correlation between the mean impact parameter of all intervenors and |RM| as these catalogs are more complete than the pure spectroscopic samples. Also, these catalogs provide the mass and star-formation rate of each galaxy which we use for our analysis. We note that the photometric galaxy catalogs include subsets of the spectrocopic catalogs. However, these catalogs do not overlap completely, which is visible in Fig. 2. Because the galaxies in the spectroscopic catalogs are chosen with certain selection criteria, it is possible that they are in general incomplete. In order to tackle this, we considered a more comprehensive sample by additionally using photometric catalogs.

3. Method

3.1. The spectroscopic sample

In order to measure the RM induced by the CGM of the intervening galaxies, we need to associate the background sources

Table 1. Properties of the background radio sources and intervenors in the spectroscopic galaxy catalogs in the COSMOS and XMM-LSS field.

Field	$N_{\rm host}$	$N_{\rm spec}$	$N_{\rm matched}$	$z_{\rm spec}$	Reference
COSMOS	111	9,022	81	0.25–0.49	Sinigaglia et al. (2022)
XMM-LSS	243	36,776	44	0.06–1.09	Basu et al. (2015)

Notes. $N_{\rm host}$ refers to the total numbers of host galaxies from the MIGHTEE sample, $N_{\rm spec}$ are the total numbers of galaxies in the spectroscopic catalogs, $N_{\rm matched}$ are the numbers of matches for the hosts, $z_{\rm spec}$ is the redshift range of the galaxies in the spectroscopic catalogs and reference is the reference paper.

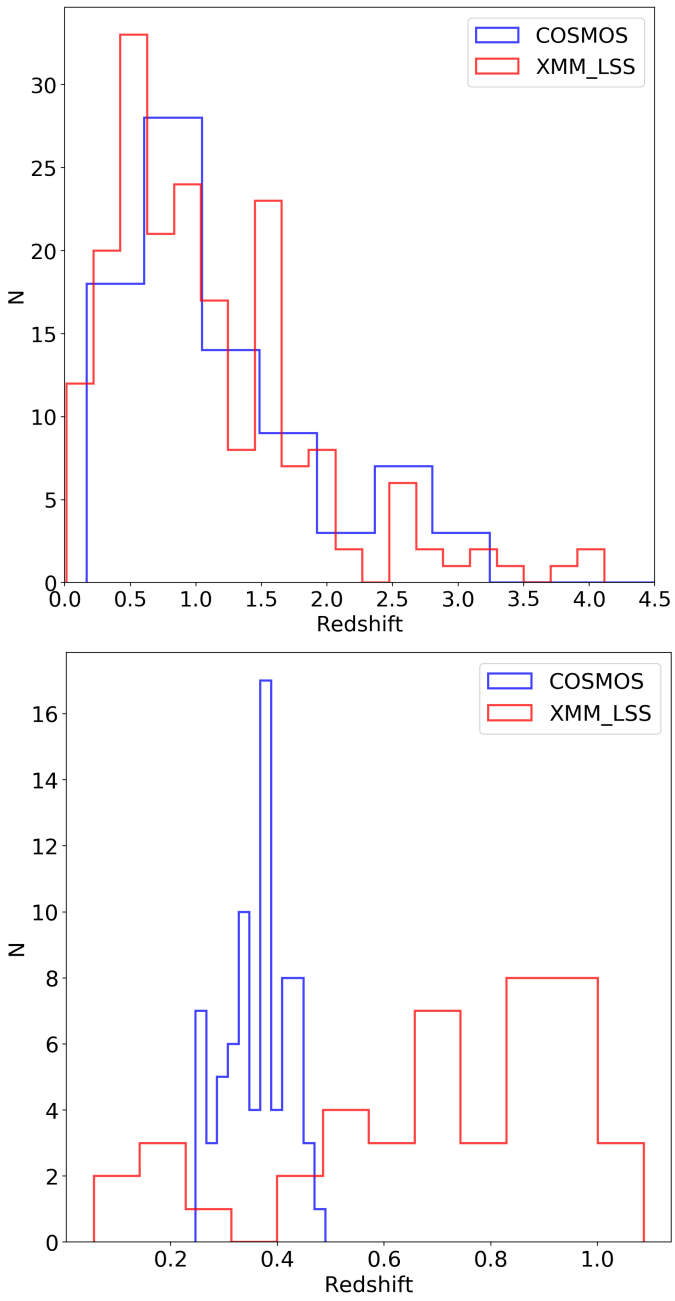

Fig. 1. Redshift distributions of host and intervening galaxies. *Upper panel*: redshift distribution of the host sources in the COSMOS field (blue) and the XMM-LSS field (red). *Lower panel*: histogram showing the redshift distribution of the 81 intervening galaxies in the COSMOS field (Sinigaglia et al. 2022) that have matched host sources within a distance of 400 kpc in blue and the redshift distribution of the 44 intervening blue cloud galaxies in the XMM-LSS field (Basu et al. 2015) that have matched host sources within a distance of 400 kpc in red.

with the intervening sources. For each background source, we search for an intervening galaxy within a projected distance of less than 400 kpc at the redshift of the intervening source. If more than one intervening galaxy matches a host source, we chose the one with the minimum central distance. We only select sources where $z_{\rm Host} > z_{\rm Intervenor}$ to ensure that the intervening galaxy lies in front of the host galaxies. For the XMM-LSS galaxy sample, we introduce a magnitude cut and exclude galaxies with $M_u > -22$ mag.

The u-band magnitude is an indicator for star-forming galaxies as the UV light is primarily emitted by hot, young, massive stars (Calzetti 2013). M_u and M_g are comparable and only differ by a value of 0.4 mag on average. Our magnitude cut does not impose any constraint on the initial catalog as the spectroscopic survey goes down to apparent magnitudes of $m_g = 27$ and an absolute magnitude of $M_g = -22$ converts to an apparent magnitude of $m_g = 23.1$ at redshift $z = 1$. This leads to the result that no galaxies in our magnitude range are cut from the catalog. In addition, by introducing the cut we select more massive galaxies which leads to more massive galactic halos which in turn may lead to a denser environments with a larger RM.

By matching the catalogs and after removing duplicates we are left with 81 (44) matches for the COSMOS (XMM-LSS) spectroscopic samples, see Table 1. As we have more volume to detect brighter galaxies at the higher redshift we add a bias by introducing a magnitude cut to our intervening galaxy sample due to the shape of the luminosity function. The redshift distributions of both samples of the intervening galaxies are shown in the lower panel of Fig. 1.

We do not correct the RM values for Galactic contamination by the Milky Way because we only look at very small patches on the sky, 1.6 deg^2 for the COSMOS field and 3.5 deg^2 for the XMM-LSS field. Hence, we expect a negligible gradient over these small sky patches and assume the contribution of the Milky Way for each field is constant over all sources and therefore not affecting our analysis. Nonetheless, we note that (Taylor et al., in prep.) found the median Galactic contribution (Galactic Rotation Measure; GRM) of the XMM-LSS field to be 8.9 ± 3.7 rad m^{-2} and of the COSMOS field to be 0.9 ± 4.1 rad m^{-2}. We note that we find fewer matches for the XMM-LSS sample, although the XMM-LSS field is larger than the COSMOS field. This is due to the introduced magnitude cut which reduces the numbers of matches from 168 to a number of 44 which is further discussed in Sect. 5.

For both of our samples, we calculate the impact parameter which is the separation between the background source and the center of the foreground galaxy in kpc. For our analysis we use the absolute value of the rotation measure, |RM|. Special care needs to be taken to compute the errors because the |RM| are an absolute quantity. The error on |RM| was calculated by assuming that the error on RM follows a Gaussian distribution. For each value of RM, we generated a random sample of |RM| drawn from an underlying Gaussian distribution, with a mean value of RM

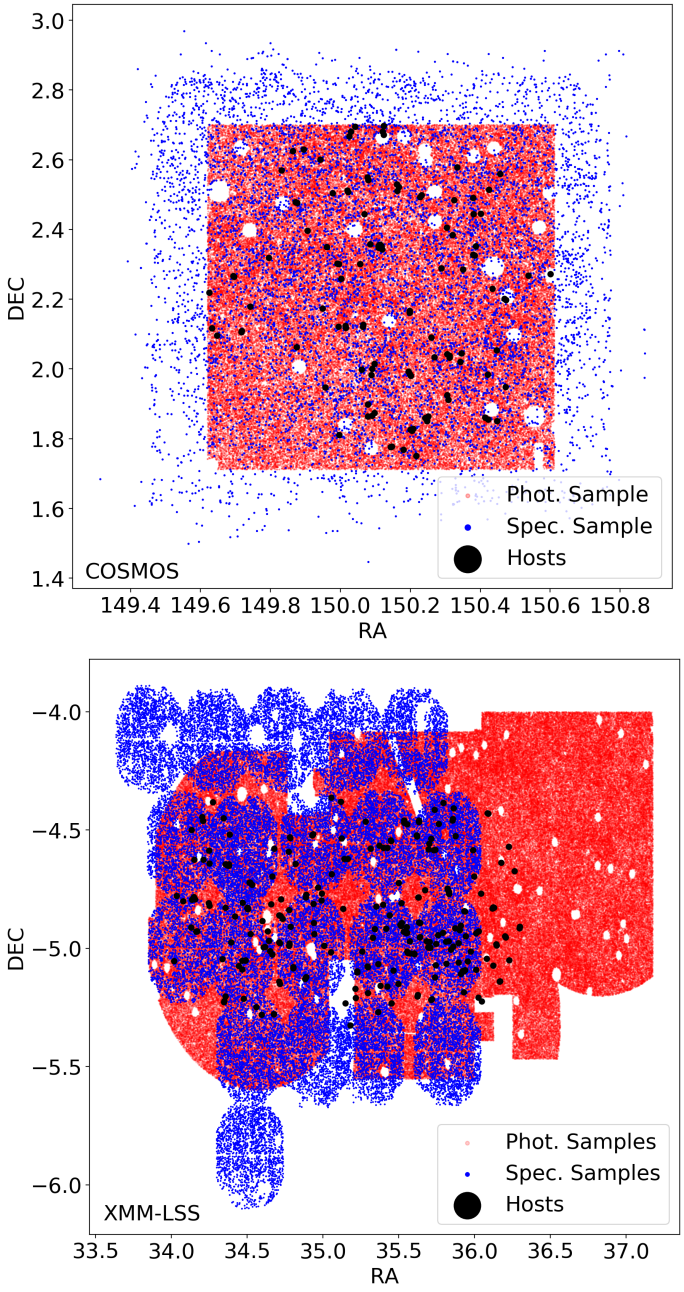

Fig. 2. Footprints of all investigated fields. *Upper panel*: we show the distribution of the intervening galaxies for the COSMOS field from the spectroscopic catalog by Sinigaglia et al. (2022) in blue and the distribution of the corresponding COSMOS MIGHTEE host galaxies in black. The intervening galaxies from the photometric (Hatfield et al. 2022) sample are shown in red. *Lower panel*: we show the distribution of the intervening galaxies for the XMM-LSS field from the spectroscopic catalog by Basu et al. (2015) in blue and the distribution of the corresponding XMM-LSS MIGHTEE host galaxies in black. The patchy distribution results from the pointings of the Inamori Magellan Areal Camera of the *Magellan* Telescope at Las Campanas Observatory. The intervening galaxies from the photometric (Hatfield et al. 2022) sample are shown in red.

and standard deviation given by the measured error on RM. We then consider the 68 percentile ($\equiv 1\sigma$) interval of the distribution of |RM|, centered at the median value of the distribution, as the error on each |RM|.

In order to investigate the excess of |RM| at smaller impact parameters, we bin the data points. For the typical mass of our galaxies, we expect a virial radius of ≈150–200 kpc. Thus, we compute three bins with an approximately equal number of objects, each with a width of 133 kpc in impact parameter. In each bin we calculate the median values of |RM| and follow the procedure of Arámburo-García et al. (2023) to estimate the error in each bin using:

$$|\mathrm{RM}|_{\mathrm{err,bin}} = \sqrt{\frac{\left\langle (x_i - \langle x \rangle)^2 \right\rangle}{n}}, \tag{4}$$

where x_i are |RM| values in each bin, $\langle x \rangle$ is their median value and n is the number of objects in each bin. We then plot the observed |RM| in rad m^{-2} vs. the impact parameter in kpc for both samples. First, we show the observed |RM| in rad m^{-2} vs. the impact parameter for the XMM-LSS without the magnitude cut of $M_u > -22$ mag of that we introduced in order to mainly select massive star-forming galaxies. As we can see in Fig. 3, this increases the number of matches of intervenors and hosts for the sample to 168 but we do not detect any excess if we also include faint galaxies with $M_u > -22$ mag.

3.2. The photometric sample

Using the spectroscopic sample, we only investigate the RM contribution from one massive, bright intervenor with the smallest impact parameter to the host. However, as the RM is an integral along the line of sight to the background radio source, we also investigate how the number of intervenors N_{int} and the mean impact parameter between a host and all its intervenors varies with the total RM of each host. The spectroscopic galaxy catalogs that we use for our analysis are incomplete in terms of magnitude and redshift and are only a subset of galaxies that lie between host and observer. In order to examine the total numbers of intervenors to each host we make use of the photometric catalogs from Hatfield et al. (2022) that contain more than 100.000 galaxies for each field to identify all intervenors to each host within a certain impact parameter.

We identify all intervening galaxies within an impact parameter of 133 kpc for each host galaxy in the two samples. We do not apply any cuts on magnitude or star-formation rate. For every host galaxy we compute the mean impact parameter to all its intervenors to investigate if there is a connection to the total |RM|. In addition, we recognize that galaxies with higher rates of star-formation are expected to exhibit stronger magnetic fields. Thus, we assume that these galaxies contribute more significantly to the total |RM| signal. We introduce a weighting scheme with respect to the impact parameter to account for the correlation between impact parameter and |RM|. The introduced weighting scheme allows us to explicitly account for the relative importance of each galaxy in the final analysis. The weighting is introduced as follows

$$\mathrm{IP}_{\mathrm{weighted,mean}} = \frac{\sum_i \mathrm{SFR}_i\, \mathrm{IP}_i}{\sum_i \mathrm{SFR}_i}, \tag{5}$$

where SFR_i is the star-formation rate and IP_i is the impact parameter in kpc of the individual intervening galaxy. Given the fact that we obtain individual impact parameters for every intervenor to the corresponding host and we only obtain a single observable value of RM which remains the same for every host, the weighting strategy must be implemented for the impact parameters. This is necessary to ensure that each individual

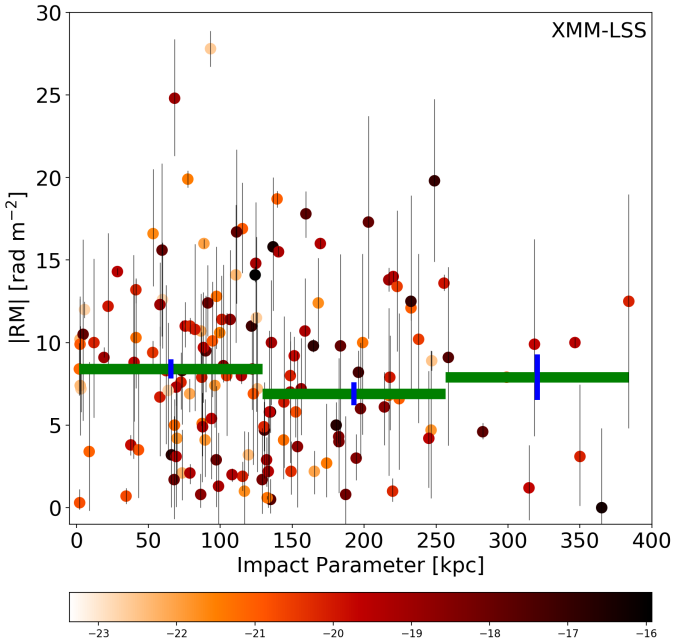

Fig. 3. Observed |RM| in rad m^{-2} vs. impact parameter in kpc for the XMM-LSS without the magnitude cut. The green bar indicates a bin of individual data points with the blue line being the error bar of the bin. The individual data points are color-coded with their corresponding u-band magnitude.

impact parameter is appropriately considered in the overall analysis, taking into account its unique contribution to the final result.

4. Results

4.1. The spectroscopic sample

Figure 4 shows the resulting plots for the spectroscopic COSMOS and XMM-LSS samples after performing the magnitude cut. For the COSMOS sample we are provided with the star formation rate (SFR), we include this information in the plot and color-code the individual data points with the SFR. For the XMM-LSS we have the individual magnitudes and we use this information in the corresponding plot for color coding the individual data points.

We calculate the absolute RM excess uncorrected for the intervening galaxies redshift. The total measured |RM| is a combination of GRM, extragalactic and noise components. The extragalactic |RM| consists of contributions from the inverveningening galaxies as well as from the foreground IGM between the source and the Milky Way as well as from contributions from the cosmic web.

For the COSMOS field that consists of a sample size of 81 we find a median |RM| of 5.9 ± 0.9 rad m^{-2} for sources with impact parameters less than 133 kpc and 3.4 ± 0.7 rad m^{-2} for sources with impact parameters greater than 133 kpc. This results in an excess of 2.5 ± 1.1 rad m^{-2}, which is significant at 2.3σ. For the XMM-LSS field that consists of a sample size of 44, the median |RM| was found to be 9.2 ± 1.4 rad m^{-2} for sources with impact parameters less than 266 kpc and 4.2 ± 1.8 rad m^{-2} for sources with impact parameters greater than 266 kpc. This corresponds to an excess of 5.0±2.3 rad m^{-2}, which is significant at 2.2σ. The median |RM| for high impact parameters of 3.4 and 4.2 rad m^{-2} with the median of the absolute value being 0.67 of the standard deviation for a Gaussian distribution. These numbers are consistent with results for the standard deviation of extragalactic sources, corrected for the Milky Way of $\sigma_{\rm RM}$ = 6 rad m^{-2} found by Schnitzeler (2010).

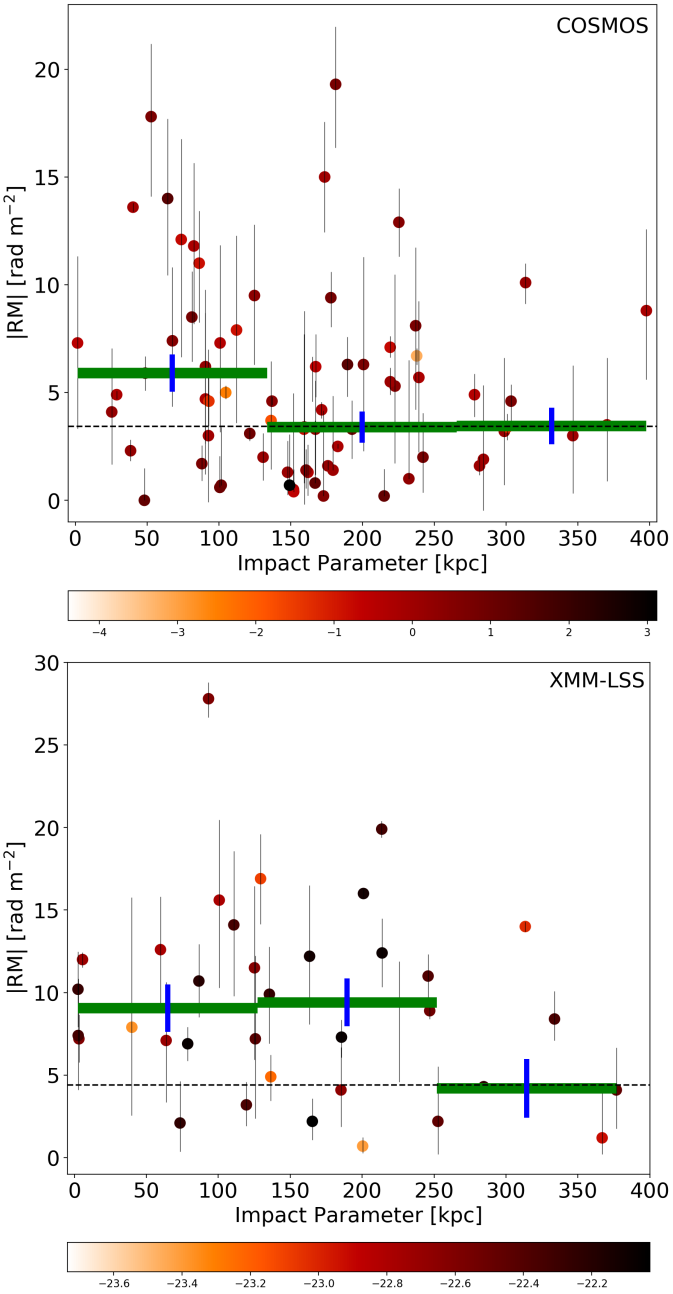

Fig. 4. Excess |RM| as function of impact parameter for the spectroscopic samples. *Upper panel*: observed |RM| in rad m^{-2} vs. impact parameter in kpc for all 81 sources in the COSMOS field. The green bar indicates a bin of individual data points with the blue line being the error bar. The data points are color-coded with respect to the star-formation rate of each galaxy. *Lower panel*: observed |RM| in rad m^{-2} vs. impact parameter in kpc for all 44 sources in the XMM-LSS field. Here, the data points are color-coded with respect to the u-band magnitude of each galaxy. For both fields all error bars show the 68% interval around |RM|.

When the samples from both fields are combined, as shown in Fig. 5, the median |RM| is found to be 7.3 ± 0.8 rad m^{-2} for sources with impact parameters less than 133 kpc and 4.3±0.9 rad m^{-2} for sources with impact parameters greater than

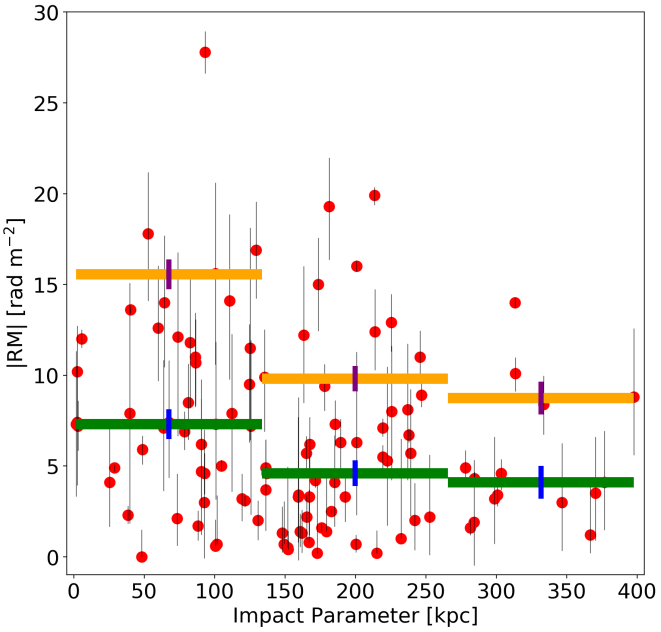

Fig. 5. Excess |RM| as function of impact parameter for the spectroscopic sample, combined for the COSMOS and XMM-LSS field. Observed |RM| in rad m^{-2} vs. impact parameter in kpc for the combination of the two samples. The green bar indicates a bin of individual data points with the blue line being the error bar of the bin. The orange bins are the redshift corrected |RM| including the error bar in purple. The error bars show the 68% interval around |RM|.

133 kpc. This results in an excess of 3.0 ± 1.2 rad m^{-2}, which is significant at 2.5σ.

As we do not have information on the individual contributions, a redshift correction would boost all contributions although they do not all occur at the same redshift. Hence, we use the redshift uncorrected measurements to investigate the |RM| in correlation with impact parameters and only perform a redshift correction on our binned results using the mean redshift of the intervenors.

We correct the |RM| excess that we found for redshift effects to get the rest frame RM:

$$\mathrm{RM}_{\mathrm{corr}} = \mathrm{RM}(1 + z_i)^2, \tag{6}$$

with z_i being the redshift of the intervenor. The median redshift for the COSMOS sample is $\bar{z}_{\mathrm{COSMOS}} = 0.37$ and for the XMM-LSS sample it is $\bar{z}_{\mathrm{XMM-LSS}} = 0.77$. If we correct the |RM| excess for redshift we now get 4.7 ± 2.1 rad m^{-2} for the COSMOS field and 15.7 ± 7.2 rad m^{-2} for the XMM-LSS field. For the combination of both samples we find a median redshift of $\bar{z}_{\mathrm{Comb}} = 0.42$ yielding to a redshift-corrected |RM| excess of 5.6 ± 2.3 rad m^{-2}. The redshift correction of the bins is also shown in Fig. 5. A two-sample Kolmogorov–Smirnov test yields a p-value of 0.01, which implies a clear significance for the excess.

We also investigate a possible connection between the |RM| of the background source and the redshift of the intervening galaxy. To this end, we compute a linear fit between |RM| and redshift. Figure 6 shows the |RM| vs. the redshift plot of each sample and the fit. In order to evaluate this correlation statistically, we perform a fit on the data and calculate the Pearson correlation coefficient to evaluate the linear correlation between the data and the fit. For the COSMOS data we get a positive trend with higher |RM| at higher redshifts and a correlation coefficient of 0.59 with a p-value of 0.12, suggesting that this trend is not

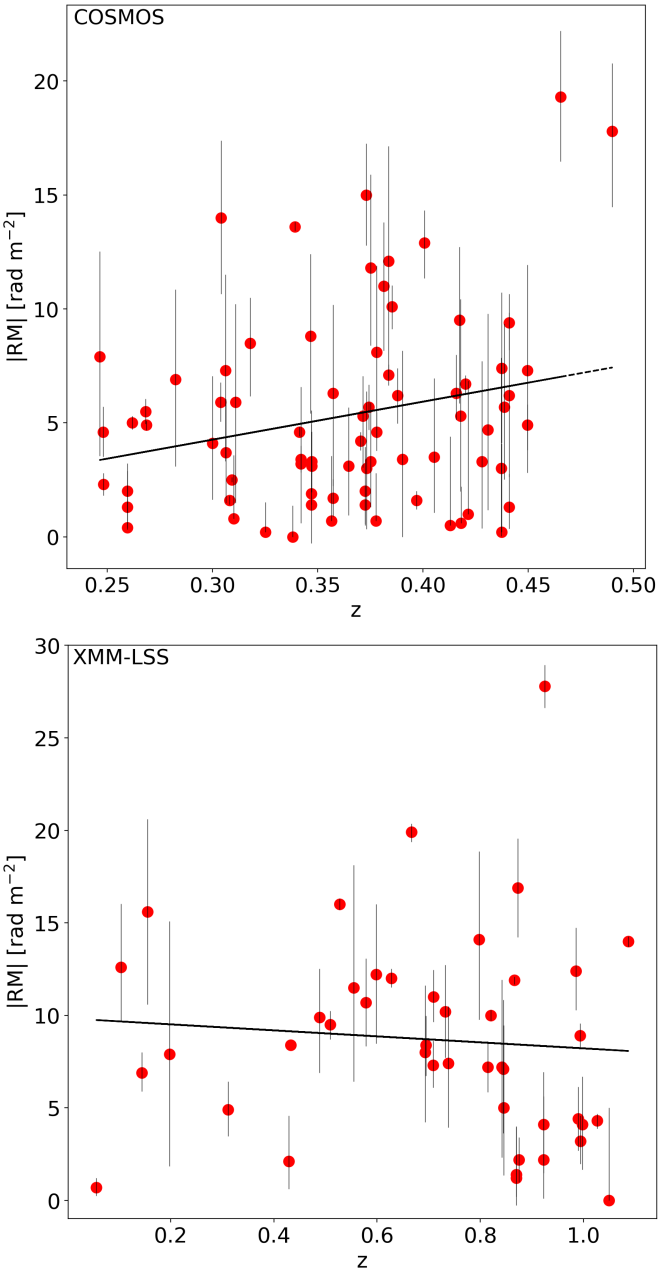

Fig. 6. |RM| as function of redshift for the spectroscopic sample. *Upper panel*: observed |RM| in rad m^{-2} vs. redshift for all 81 sources in the COSMOS field. The black line represents the best fit including all data points. *Lower panel*: observed |RM| in rad m^{-2} vs. redshift for all 44 sources in the XMM-LSS field. Again, the black line represents the best fit. For both fields all error bars show the 68% interval around |RM|.

significant. In contrast, the results for the XMM-LSS field indicate a negative trend with a declining |RM| toward higher redshifts. However, we note that the Pearson correlation coefficient yields 0.05 for this sample with a p-value of 0.9. So we do not detect a correlation between |RM| and redshift for the XMM-LSS but we see an indication for a positive correlation for the COSMOS sample.

4.2. The photometric sample

We plot the mean impact parameter of each host to all its intervenors vs. |RM| treating all intervenors equally in Fig. 7. In

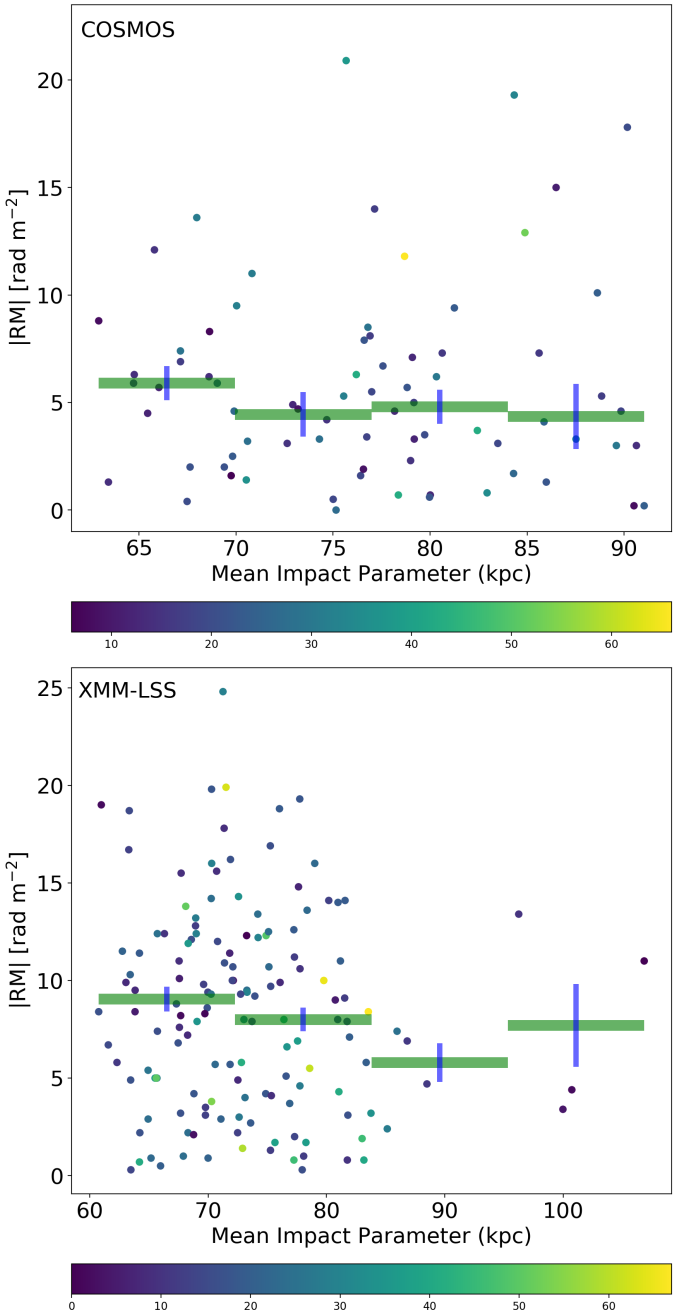

Fig. 7. |RM| as function of mean impact parameter for the photometric sample. *Upper panel*: we plot the observed |RM| in rad m^{-2} vs. the mean impact parameter of all intervening galaxies within 133 kpc around the host from the photometric catalog provided by Hatfield et al. (2022) for the COSMOS field. The green bar indicates a bin of individual data points with the blue line being the error bar of the bin. The individual data points are color-coded with respect to the total number of intervenors to each host. *Lower panel*: corresponding plot for the XMM-LSS field.

addition, we color-code the individual data points with respect to the total number of intervenors $N_{\rm int}$ to each host to investigate a possible correlation between $N_{\rm int}$ and |RM|. The number of intervenors to each host within an impact parameter of 133 kpc reach from $6 < N_{\rm int} < 66$ with the median being $\langle N_{\rm int}\rangle = 20$ for the COSMOS field, and $6 < N_{\rm int} < 67$ with the median being $\langle N_{\rm int}\rangle = 18$ for the XMM-LSS field. The total numbers from the photometric catalog are presented in Table 2. We investigate the correlation between the mean impact parameter to the total |RM| by binning the data. Again, we calculate the error of each bin as it is described in Eq. (4). Inspecting the data in terms of $N_{\rm int}$ does not yield any correlation between the total number of intervenors $N_{\rm int}$ to the total |RM|. Binning the data does not lead to definitive results or trends for either sample. However, caution is necessary when interpreting the data, particularly in cases where the bins with larger impact parameters include only few data points. The absolute magnitudes of the intervenors are in the range of $-20.1\,\text{mag} < M_g < -12.1\,\text{mag}$ with a median of $\langle M_g\rangle = -15.5\,\text{mag}$ for the XMM-LSS field and of $-18.9\,\text{mag} < M_g < -13.8\,\text{mag}$ with a median of $\langle M_g\rangle = -14.8\,\text{mag}$ for the COSMOS field. This means that the galaxies in the photometric sample go down to much lower brightness than in the spectroscopic sample with a magnitude cut in the u-band. Even though the photometric catalogs includes most of the galaxies from the spectroscopic samples, including a large number of faint galaxies to contribute to the RM leads to a dilution of the central RM excess seen for the bright galaxies in the spectroscopic sample.

Evidently, the photometric catalog extends to larger redshifts than the spectroscopic catalog. Since we use the redshift of each intervenor to calculate the impact parameter, we also propagate the error to the impact parameter calculation. The mean redshift of the intervenors in the two catalogs is $\langle z_{\rm int}\rangle = 0.26$ with a mean error on the photometric redshifts of $\langle z_{\rm err}\rangle \sim 0.08$ (Hatfield et al. 2022) which yields an impact parameter error of ±30 kpc on average.

Next, we re-compute the mean impact parameter of each host to all its intervenors vs. the total |RM| applying a weighting by the star-formation rate introduced in Eq. (5). The weighting scheme takes into account the intervenors' star-formation rate and we assume that intervenors with higher star formation rates contribute more to the |RM|. In Fig. 8 we show the resulting plot. Again, in both samples, we do not find any excess of |RM| at smaller impact parameters.

5. Discussion

5.1. The spectroscopic sample

We detect of an excess of |RM| for small impact parameters in both MIGHTEE fields. The COSMOS sample shows an excess at a radius below 133 kpc around the galaxy whereas the XMM-LSS exhibits an excess up to a radius of 266 kpc. The higher median redshift of the XMM-LSS sample would suggest that also the virial radius of these galaxies is larger as we are biased to more massive systems at higher redshift which is in agreement with our results. We note that we detect the excess in the XMM-LSS sample only if we introduce a magnitude cut for intervenors with $M_u > -22$ mag. Thus, we only select massive galaxies with a denser CGM at a fixed distance. In addition, these galaxies are assumed to have higher star formation rates and therefore higher RM since star formation can drive magnetized outflows on galactic scales (Wiener et al. 2017; Basu et al. 2018). The XMM-LSS sample is more inhomogenous than the COSMOS sample because of the wider redshift range and hence any excess at small impact parameters may be less obvious. The redshift-corrected excess from the combined samples is 3.0 ± 1.2 rad m^{-2}, which is significant at 2.5σ.

The increase toward small impact parameters of the |RM| is consistent with previous results suggesting the presence of significant magnetic fields in and around galaxies at distances of several tens of kpc (Bernet et al. 2008, 2012, 2013). However, we find that our results are lower than found in some

Table 2. Properties of the photometric galaxy catalog from Hatfield et al. (2022) and the median properties of the intervenors we find to the host sample.

Field	$N_{\rm host}$	$N_{\rm photometric}$	$\langle N_{\rm int}\rangle$	$\langle z_{\rm phot,int}\rangle$	$\langle M_{g,\rm int}\rangle$ (mag)	$\langle m_{\rm int}\rangle$ $\log_{10}(M_\odot)$	$\langle {\rm SFR}_{\rm int}\rangle$ $\log_{10}(M_\odot\,{\rm yr}^{-1})$
COSMOS	111	125 676	20	0.26	−14.8	8.1	−10.1
XMM-LSS	243	384 354	18	0.22	−15.5	7.8	−12.2

Notes. $N_{\rm host}$ are the total numbers of host galaxies from the MIGHTEE sample, $N_{\rm photometric}$ are the total numbers of galaxies in the photometric catalog for each field, $\langle N_{\rm int}\rangle$ is the median number of intervenors for each host, $\langle z_{\rm phot,int}\rangle$ is the median redshift of the intervenors, $\langle M_{g,\rm int}\rangle$ is the median M_g magnitude of the intervenors, and $\langle m_{\rm int}\rangle$ and $\langle {\rm SFR}_{\rm int}\rangle$ are the median mass and star-formation rate of all intervenors in $\log_{10}(M_\odot)$ and $\log_{10}(M_\odot\,{\rm yr}^{-1})$ respectively.

previous work. Farnes et al. (2014) found an excess in |RM| of $24 \pm 6\,{\rm rad\,m^{-2}}$ in Mg II absorbers and Bernet et al. (2008) found an excess of $140\,{\rm rad\,m^{-2}}$. However, more recently, Heesen et al. (2023) used LOFAR observations to investigate a sample of nearby galaxies and found an excess in |RM| of $3.7\,{\rm rad\,m^{-2}}$ with an uncertainty between $\pm 0.9\,{\rm rad\,m^{-2}}$ and $\pm 1.3\,{\rm rad\,m^{-2}}$ corresponding to a significance of 2.8σ–4.1σ which is in agreement with our results. We note that Heesen et al. (2023) detected the excess of |RM| only for galaxies along the minor axis of inclined galaxies. For our samples at much higher redshifts, we cannot test this since we have no information about the orientation or inclination. Our data leads to a significance level of 2.5σ for the combination of both fields.

From our data, we can estimate the number of detections that we would need to get to a more reliable 3σ significance detection level. As σ scales with $\sqrt{n}$ and with given $n_{2.5\sigma} = 125$ (current combined sample size), the sample size that we would need for a 3σ detection is estimated to be $n_{3\sigma} = 180$.

Another possibility to increase the significance that would not need as many new detections, would be to build a cleaner sample of hosts. For example, if the background hosts consisted of AGN in clusters then these hosts would have a larger intrinsic scatter in |RM| compared to hosts in poor group or isolated environments. Ideally, the background sources would only consist of AGN with a minimal contribution to the overall |RM| scatter. Alternatively, a weighting scheme could be introduced in order to account for the different underlying populations (Rudnick 2019).

We do not find a connection between redshift and |RM| which could be due to following reasons: As the XMM-LSS sample has a much higher redshift range ($0.06 < z < 1.09$) than the COSMOS sample ($0.25 < z < 0.46$), the trend of the XMM-LSS sample provides an indication over a wider redshift range. However, the explicitly high redshift detections of the XMM-LSS lead to the fact that more intervening material occurs along the line of sight and the sample becomes more scrambled. In contrast, the smaller redshift range of the COSMOS sample leads to a more homogeneous sample so the results derived from this sample has more significance compared to the more heterogenous XMM-LSS sample. We note that there are two outliers showing high |RM| and high redshift. To test if the positive correlation is only due to those outliers, we mask these two outliers and compute the correlation again. As a result, we still detect a positive trend but with a shallower slope.

Previous work found contradictory results. Work by Kronberg & Perry (1982), Welter et al. (1984) and Kronberg et al. (2008) have found an increased |RM| at higher redshifts. More recent work by Hammond et al. (2012), Bernet et al. (2012) and Pshirkov et al. (2016) did not find any significant evidence for a correlation between |RM| and redshift. We note that the studies that find a positive correlation between |RM| and redshift have been carried out before the release of the reanalyzed NRAO VLA Sky Survey (NVSS) RM catalog (Taylor et al. 2009; Oppermann et al. 2012). The more recent work that does not find a correlation between |RM| and redshift used the improved NVSS RM catalog.

In order to determine the magnitude of the magnetic field strength around galaxies, we use Eq. (3). Assuming an electron density of $n_{\rm e} \approx 10^{-4}\,{\rm cm^{-3}}$ and a line-of-sight length of $\approx$100 kpc we estimate a magnetic field strength of $B \approx 0.48\,\mu{\rm G}$ for the redshift corrected and combined sample. We note that this result is only a lower limit because the magnetic field strength may be amplified as magnetic field reversals can lower the RM.

The magnetic field strength in the disks of galaxies is usually found to be of order 10–15 μG (Pakmor et al. 2017). Observations of nearby galaxies show that the magnetic field can be described by $B = B_0 \exp(-r/r_0)$ (Beck 2015). Assuming magnetic fields to go down following the above relation from the galactic disk to CGM, and $B_0 \approx 10\,\mu{\rm G}$ and $r_0 \approx 10\,{\rm kpc}$ we derive $B = 0.45\,\mu{\rm G}$ at a distance of 100 kpc from the galaxies center. Simulations suggest similar values for the magnetic field strength around galaxies (Pakmor et al. 2020). Heesen et al. (2023) found a magnetic field strength of $\approx$0.50 μG for a sample of nearby galaxies. This agrees with our estimate which is derived from a sample of galaxies at higher z and with higher SFR.

5.2. The photometric sample

In the preceding analysis of the spectroscopic catalog, we assumed that the contribution to the RM is dominated by one massive and bright intervenor with the smallest impact parameter to the LOS to the host. However, our host are located at high redshifts, resulting in a large number of intervening galaxies. Not all galaxies contribute equally to the observed RM. We expect that those with higher masses or higher star-formation rates tend to exhibit stronger magnetic fields in the CGM. Previous studies that examined the RM around galaxies neglected the effect of multiple intervenors.

Using the photometric catalog from Hatfield et al. (2022) allows us to assess the effect of multiple intervenors on the RM. In addition, by implementing various weighting schemes, we can investigate if galaxies with higher masses or star-formation rates have a greater influence on the RM. In this work, we introduced a weighting scheme that takes into account the star-formation rate of each galaxy. Our initial hypothesis suggests that the RM generated by intervenors is higher when they exhibit higher star-formation rates and if they are located at smaller impact parameters. While our analysis provides some preliminary evidence to support this assumption, we cannot draw any definitive conclusions due to the limitations of the available data. The spectroscopic sample indicates that an excess of |RM| is detected

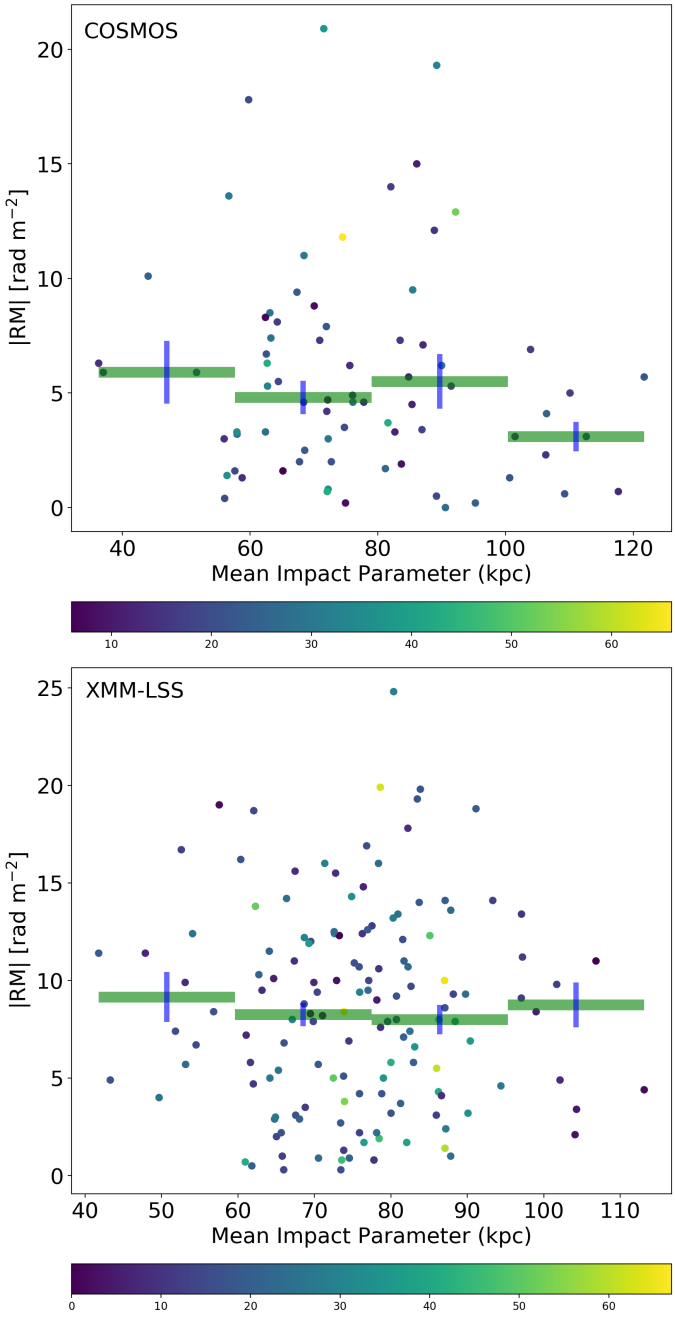

Fig. 8. |RM| as function of weighted mean impact parameter for the photometric sample. *Upper panel*: we plot the observed |RM| in rad m^{-2} vs. the weighted median impact parameter in kpc from the photometric catalog provided by Hatfield et al. (2022) within an impact parameter of 133 kpc around each host for the COSMOS field. The green bar indicates a bin of individual data points with the blue line being the error bar of the bin. The individual data points are color-coded with respect to the total number of intervenors to each host. *Lower panel*: corresponding plot for the XMM-LSS field.

at smaller impact parameters, which fall within the size range of the circumgalactic medium (CGM) when considering only the most luminous galaxy. However, using the photometric sample, we observe only a small trend between the average impact parameter and the |RM|. As a result, we infer that the most luminous galaxy is most likely the primary contributor to the overall RM.

6. Conclusions

Magnetic fields around galaxies are important to understand galaxy evolution as they regulate the transport of cosmic rays. Direct observations of the CGM are limited to a few nearby sources as the CGM is very tenuous. Indirect methods such as transverse absorption-line studies are therefore a powerful tool to investigate the physical conditions in the CGM such as the metallicity, temperature and gas density and also the magnetic field strength.

We used MIGHTEE-POL data to measure the RM around foreground star-forming galaxies to investigate the strength of magnetic fields in the CGM. We used catalogs of star-forming and blue cloud galaxies to measure the rotation measure of MIGHTEE-POL sources as a function of the impact parameter from the intervening galaxy and derived the magnetic field strength of the CGM. Also we investigated a possible connection between the |RM| and the redshift. In addition, we studied the impact of all intervenors along the line of sight using the photometric catalogs from Hatfield et al. (2022) with respect to the mean impact parameter. To account for the impact of mass and star-formation rate of the individual intervenors we introduced a weighting scheme.

In summary, we can draw the following conclusions:

1. For a sample with high star-forming galaxies in the MIGHTEE-POL survey by MeerKAT in the XMM-LSS and COSMOS fields we find an excess of the RM for impact parameters of less than 133 kpc around bright spectroscopic galaxies with a significance of 2.5σ. We attribute this excess to coherent magnetic fields in the CGM. The excess RM is in agreement with recent work of Heesen et al. (2023) for nearby galaxies, but lower than previous work (Bernet et al. 2013; Farnes et al. 2014). We do not subtract the contribution of the Galactic RM.
2. For a complete sample including galaxies down to magnitudes of $M_g \approx -13.8$, we do not find any RM excess which suggests that only bright, star-forming galaxies with impact parameters less than 130 kpc significantly contribute to the RM of the background radio source.
3. Making rough assumptions on the electron density in the CGM, we estimate the magnetic field strength to be of the order of $B = 0.5\,\mu$G which is in agreement with observations and simulations.
4. We do not find a correlation between the RM of intervening galaxies and their redshift.
5. Using the photometric catalog we do not find a correlation between the total number of intervenors, $N_{\rm int}$, to the total |RM|. Even introducing a weighting scheme that takes into account the star-formation rate does not lead to an |RM| excess in the innermost bin.

Our results suggest that there is a correlation between the impact parameter and the rotation measure which indicates the presence of intervening magnetic fields in the CGM. We find that the |RM| becomes smaller with higher impact parameters for both our samples. Future studies with larger catalogs of background quasars and more accurate RM measurements enable extensive and more detailed studies of the magnetized CGM.

Below we summarize the main caveats of our work:

1. Selection function of foreground galaxies: The galaxy catalogs that are used are complete in terms of magnitude but not volume-limited. Even though the RM from galaxies at higher z contribute less, there may be still undetected intervening galaxies. Certainly for the XMM-LSS field the coverage is not uniform across the field.

2. The total RM is an integral along the line of sight and we cannot differentiate between contributions from the host, other intervenors or Galactic contributions. Advanced techniques such as rotations measure synthesis can be useful here.

In our work we make use of early-release data from MIGHTEE-POL which is characterized by a relatively high level of uncertainty. Still we could extract statistically significant signals from this early-release data. MIGHTEE serves as a pilot study for surveys with the forthcoming Square Kilometre Array (SKA). Therefore, our results can soon be tested with much larger data sets. The polarization Sky Survey of the Universe's Magnetism (POSSUM) carried out by ASKAP, for example, will map a large area of the sky and it is expected to detect millions of rotations measures. Larger catalogs will yield a more robust detection of magnetic fields in the CGM. Prospects for future work also include the study of the CGM of quiescent galaxies, where synchrotron emission due to star formation activity is absent.

Acknowledgements. The authors thank the anonymous referee for useful comments and suggestions. The MeerKAT telescope is operated by the South African Radio Astronomy Observatory, which is a facility of the National Research Foundation, an agency of the Department of Science and Innovation. We acknowledge use of the Inter-University Institute for Data Intensive Astronomy (IDIA) data intensive research cloud for data processing. IDIA is a South African university partnership involving the University of Cape Town, the University of Pretoria and the University of the Western Cape. The authors acknowledge the Centre for High Performance Computing (CHPC), South Africa, for providing computational resources to this research project. KB and MB acknowledge funding by the Deutsche Forschungsgemeinschaft (DFG, German Research Foundation) under Germany's Excellence Strategy – EXC 2121 "Quantum Universe" – 390833306. KB and MB thank Francesco Sinigaglia and collaborators for providing the catalog used in Sinigaglia et al. 2022. MNT acknowledges support from the Oxford Hintze Centre for Astrophysical Surveys which is funded through generous support from the Hintze Family Charitable Foundation. NJA acknowledges support from the ERC Advanced Investigator Grant EPOCHS (788113). RB acknowledges support from an STFC Ernest Rutherford Fellowship (grant number ST/T003596/1). SPO acknowledges support from the Comunidad de Madrid Atracción de Talento program via grant 2022-T1/TIC-23797.

References

Aihara, H., Arimoto, N., Armstrong, R., et al. 2018, PASJ, 70, S4
Akahori, T., Ryu, D., & Gaensler, B. M. 2016, ApJ, 824, 105
Arámburo-García, A., Bondarenko, K., Boyarsky, A., et al. 2023, MNRAS, 519, 4030
Basu, A., Wadadekar, Y., Beelen, A., et al. 2015, ApJ, 803, 51
Basu, A., Mao, S. A., Fletcher, A., et al. 2018, MNRAS, 477, 2528
Beck, R. 2015, A&ARv, 24, 4
Beck, R., Brandenburg, A., Moss, D., Shukurov, A., & Sokoloff, D. 1996, ARA&A, 34, 155
Bernet, M. L., Miniati, F., Lilly, S. J., Kronberg, P. P., & Dessauges-Zavadsky, M. 2008, Nature, 454, 302
Bernet, M. L., Miniati, F., & Lilly, S. J. 2010, ApJ, 711, 380
Bernet, M. L., Miniati, F., & Lilly, S. J. 2012, ApJ, 761, 144
Bernet, M. L., Miniati, F., & Lilly, S. J. 2013, ApJ, 772, L28
Calzetti, D. 2013, Secular Evolution of Galaxies (Cambridge: Cambridge University Press), 419
Carretti, E., O'Sullivan, S. P., Vacca, V., et al. 2023, MNRAS, 518, 2273
Davies, L. J. M., Robotham, A. S. G., Driver, S. P., et al. 2018, MNRAS, 480, 768
DeFelippis, D., Bouché, N. F., Genel, S., et al. 2021, ApJ, 923, 56
Donahue, M., & Voit, G. M. 2022, Phys. Rep., 973, 1
Farnes, J. S., O'Sullivan, S. P., Corrigan, M. E., & Gaensler, B. M. 2014, ApJ, 795, 63
Fletcher, A., Beck, R., Shukurov, A., Berkhuijsen, E. M., & Horellou, C. 2011, MNRAS, 412, 2396
Hammond, A. M., Robishaw, T., & Gaensler, B. M. 2012, arXiv e-prints [arXiv:1209.1438]
Hatfield, P. W., Jarvis, M. J., Adams, N., et al. 2022, MNRAS, 513, 3719
Heesen, V., O'Sullivan, S. P., Brüggen, M., et al. 2023, A&A, 670, L23
Heywood, I., Jarvis, M. J., Hale, C. L., et al. 2022, MNRAS, 509, 2150
Jarvis, M. J., Häußler, B., & McAlpine, K. 2013, The Messenger, 154, 26
Jarvis, M., Taylor, R., Agudo, I., et al. 2016, MeerKAT Science: On the Pathway to the SKA, 6
Kacprzak, G. G., Churchill, C. W., Steidel, C. C., & Murphy, M. T. 2008, AJ, 135, 922
Kim, K. S., Lilly, S. J., Miniati, F., et al. 2016, ApJ, 829, 133
Kronberg, P. P., & Perry, J. J. 1982, ApJ, 263, 518
Kronberg, P. P., Bernet, M. L., Miniati, F., et al. 2008, ApJ, 676, 70
Lan, T.-W., & Prochaska, J. X. 2020, MNRAS, 496, 3142
Machado, R. E. G., Tissera, P. B., Lima Neto, G. B., & Sodré, L. 2018, A&A, 609, A66
Maddox, N., Frank, B. S., Ponomareva, A. A., et al. 2021, A&A, 646, A35
Mao, S. A., Carilli, C., Gaensler, B. M., et al. 2017, Nat. Astron., 1, 621
Mintz, A., Jorgenson, R., & Rafelski, M. 2020, Bull. Am. Astron. Soc., 235, 205.06
Miskolczi, A., Heesen, V., Horellou, C., et al. 2019, A&A, 622, A9
Oppermann, N., Junklewitz, H., Robbers, G., et al. 2012, A&A, 542, A93
Oren, A. L., & Wolfe, A. M. 1995, ApJ, 445, 624
O'Sullivan, S. P., Shimwell, T. W., Hardcastle, M. J., et al. 2023, MNRAS, 519, 5723
Pakmor, R., Gómez, F. A., Grand, R. J. J., et al. 2017, MNRAS, 469, 3185
Pakmor, R., van de Voort, F., Bieri, R., et al. 2020, MNRAS, 498, 3125
Péroux, C., Nelson, D., van de Voort, F., et al. 2020, MNRAS, 499, 2462
Pierre, M., Valtchanov, I., Altieri, B., et al. 2004, J. Cosmol. Astropart. Phys., 2004, 011
Pillepich, A., Nelson, D., Truong, N., et al. 2021, MNRAS, 508, 4667
Pomakov, V. P., O'Sullivan, S. P., Brüggen, M., et al. 2022, MNRAS, 515, 256
Pshirkov, M. S., Tinyakov, P. G., & Urban, F. R. 2016, Phys. Rev. Lett., 116, 191302
Rudnick, L. 2019, arXiv e-prints [arXiv:1901.09074]
Schnitzeler, D. H. F. M. 2010, MNRAS, 409, L99
Scoville, N., Aussel, H., Brusa, M., et al. 2007, ApJS, 172, 1
Sekhar, S., Jagannathan, P., Kirk, B., Bhatnagar, S., & Taylor, R. 2022, AJ, 163, 87
Sinigaglia, F., Rodighiero, G., Elson, E., et al. 2022, ApJ, 935, L13
Taylor, A. R., Stil, J. M., & Sunstrum, C. 2009, ApJ, 702, 1230
Thomas, T., Pfrommer, C., & Pakmor, R. 2022, MNRAS, submitted [arXiv:2203.12029]
Tumlinson, J., Peeples, M. S., & Werk, J. K. 2017, ARA&A, 55, 389
Vacca, V., Oppermann, N., Enßlin, T., et al. 2016, A&A, 591, A13
Weaver, J. R., Kauffmann, O. B., Ilbert, O., et al. 2022, ApJS, 258, 11
Welter, G. L., Perry, J. J., & Kronberg, P. P. 1984, ApJ, 279, 19
Wiener, J., Pfrommer, C., & Oh, S. P. 2017, MNRAS, 467, 906